TECHNICAL MEMORANDUM

353

Large scale non-turbulent dynamics in the atmosphere

M.J.P. Cullen

Research Department

Submitted for publication in Q. J. Roy. Met. Soc.

November 2001

European Centre for Medium-Range Weather Forecasts
Europäisches Zentrum für mittelfristige Wettervorhersage
Centre européen pour les prévisions météorologiques à moyen terme

For additional copies please contact

The Library
ECMWF
Shinfield Park
Reading
RG2 9AX
library@ecmwf.int

Series: ECMWF Technical Memoranda

A full list of ECMWF Publications can be found on our web site under:
http://www.ecmwf.int/pressroom/publications/

Abstract

Classical two-dimensional turbulence theory is often used to understand large scale atmospheric flows. However, the equations governing classical two-dimensional turbulence can only be derived from quasi-geostrophic theory by assuming that the horizontal scale is much smaller than the deformation radius, which is the scale on which baroclinic instability takes place. Typically, the large scale quasi-two-dimensional disturbances have the vertical depth scale of the troposphere and are of larger scale than the baroclinic waves which maintain them. It is therefore more appropriate to study the quasi-two-dimensional disturbances with a model appropriate to scales larger than the deformation radius. The simplest example of such a model is the equivalent barotropic model. The semi-geostrophic model is also accurate in this regime, but more general. We show that it does not permit the enstrophy cascades associated with classical two-dimensional turbulence. This agrees with other results in the literature suggesting that two-dimensional flow on scales larger than the deformation radius is essentially non-turbulent. The observed quasi-permanently unsteady behaviour of the atmosphere thus represents the natural internal dynamics, and does not require explanation by anisotropic forcing. In the ocean, on the other hand, the external deformation radius, which governs the behaviour of two-dimensional eddies, is much larger than the internal deformation radius, which determines the scale of baroclinic development. It may thus be appropriate to use two-dimensional turbulence as a model for scales between the internal and external deformation radius.

1 Introduction

It is a matter of common observation that the motion of the atmosphere, on scales of the size represented on traditional weather maps, exhibits permanent unsteadiness. However, the statistics of the flow are rather constant, in that a similar number of disturbances are always present at a given season of the year. The question is whether the large-scale transient behaviour is best treated as a forced-dissipative system, in which the atmosphere would speedily relax to a symmetric state if the forcing was removed, or whether there can be a natural unsteady evolution which would persist for long times in the absence of forcing or dissipation. Much work has concentrated on the former, such as the pioneering work of Charney and Devore (1979) illustrating the effect of topography in creating large-scale disturbances. An alternative view is the Hamiltonian approach, which assumes that there are time-scales long enough for obviously dissipative events such as convection not to be dominant, but shorter than the characteristic time-scales of radiative forcing and frictional spin-down. It is then possible to model the evolution by equations which conserve energy.

This paper considers various Hamiltonian models. These are illustrated in Fig.1, which shows a hierarchy of models derived from the three-dimensional Navier-Stokes equations under various scaling assumptions.

The most elementary relevant model is that of two-dimensional incompressible flow. Leith (1971) showed that this model gives a k^{-3} energy spectrum which is consistent with observations of the large-scale flow, Gage and Nastrom (1986). This model predicts a systematic cascade of energy to the largest scales and enstrophy to the smallest scales. The latter property means that dissipation is required in computer simulations, even though the mathematical results, e.g. Kato and Ponce (1986), show that solutions stay smooth for infinite time given smooth initial data. Though the equations can be integrated in either direction in time, there is irreversibility in the flow, characterised by the filamentation of the vorticity field. The behaviour of the model is somewhat different if it is applied on a rotating spherical surface. Filamentation is not prevented, but the upscale energy cascade in meridional wavenumber is limited by the beta effect, giving typical solutions for vorticity which are arbitrary monotonic functions of latitude but independent of longitude. A review of these issues is given by Holloway (1986).

Charney (1971) showed that the three-dimensional quasi-geostrophic equations could be used to predict qualitatively similar behaviour to that of two-dimensional incompressible flow in a stratified fluid. However, this

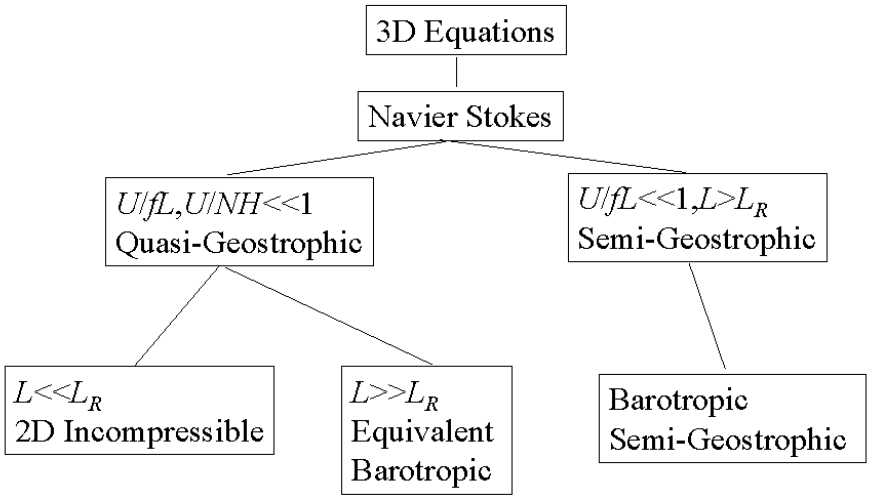

Figure 1: The hierarchy of equations approximating the three-dimensional Navier-Stokes equations that are used in this paper. L, H are horizontal and vertical length scales, U a velocity scale, f the Coriolis parameter and N the Brunt-Vaisala frequency. L_R is the deformation radius NH/f.

is only the case for horizontal scales smaller than the deformation radius L_R. Thus the upscale energy transfer would not necessarily destroy non-zonal perturbations of scales larger than L_R. Larichev and McWilliams (1991) and Farge and Sadourny (1989) have studied the 'turbulence' of two-dimensional models appropriate to scales larger than L_R and found a much more stationary spectrum and weaker cascades. This is consistent with the observed unsteady non-zonal behaviour of the troposphere and the more zonal behaviour of the stratosphere where L_R is greater. In the ocean the situation is rather different, because the external deformation radius felt by barotropic eddies is much larger than the internal deformation radius on which baroclinic disturbances grow. Thus the two-dimensional incompressible model may be more relevant in the ocean.

There is extensive theory of the equations of two-dimensional incompressible flow because the Lagrangian conservation of vorticity strongly constrains the solutions. There is much less theory for the equivalent barotropic model obtained as the asymptotic limit of the quasi-geostrophic potential vorticity equation for scales larger than L_R. This is because the equation is less amenable to analysis. The dynamics of this regime have thus received much less attention.

Cullen (2000) showed that the semi-geostrophic model was accurate for scales larger than L_R, and it is also amenable to analysis. We therefore use a barotropic version of this model on the f-plane to study the regime $L > L_R$. We demonstrate by computation that the model does not produce cascades to small scales. It only appears to permit algebraic growth of line elements. This does not prevent the growth of spiral structures in potential vorticity, as discussed by Methven and Hoskins (1998), but does prevent the exponential growth of potential vorticity filaments observed in two-dimensional turbulence. The resulting flow is therefore more 'reversible' than classical two-dimensional turbulence. We also derive theoretical results that show why the cascade is inhibited, though it is not possible to exclude local regions of exponential growth.

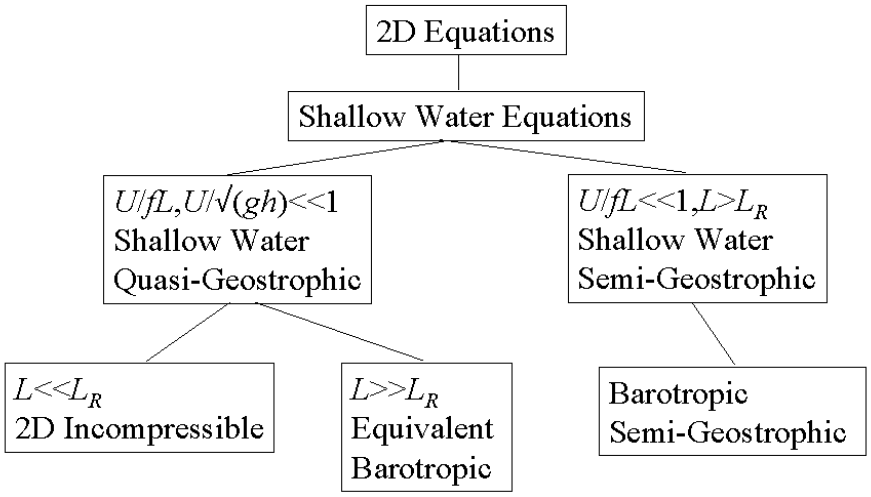

Figure 2: The hierarchy of equations approximating the shallow water equations that are used in this paper. Notation as Fig.1, with g being the acceleration due to gravity and h the mean depth.

The scaling required for semi-geostrophic theory to be accurate only requires one horizontal length scale to be large compared with L_R. Thus it is valid for filaments which are not sharply curved. In the example shown by Methven and Hoskins (1998), the depth of potential vorticity filaments reaches 4km, requiring an along-filament scale greater than 400km (i.e. a wavelength greater than 2500km) for semi-geostrophic theory to be accurate. The theory will not be reliable for studying the instability of the filaments, which will typically generate length scales smaller than L_R in both directions. Methven and Hoskins show examples of such instabilities, and the issue is also discussed by Malardel et al. (1993) in the context of the instability of a filament of potential vorticity associated with a front. The lack of cascades in semi-geostrophic solutions at smaller scales than L_R represents a symptom of the inaccuracy of the approximation, and does not indicate that there are no real cascades or consequent efficient mixing. However, the theory is relevant for study of the persistence of non-zonal eddies in the atmospheric circulation, since these are on scales similar to or larger than L_R. It is also relevant for studying long-lived, i.e. stable, filamentary structures.

2 Two-dimensional turbulence in the atmosphere

2.1 Quasi-geostrophic theory

The classical theory was originally set out in three dimensions by Charney (1971). In this paper we consider various approximations in the context of the shallow water equations, as illustrated in Fig.2.

The quasi-geostrophic shallow water equations on a domain $\Gamma(x,y)$ with boundary $\partial\Gamma$ can be written

$$\begin{aligned} \frac{Dq}{Dt} &= 0 \\ \mathbf{u} &= (-\frac{\partial \psi}{\partial y}, \frac{\partial \psi}{\partial x}) \\ q - f &= gh_0 \nabla^2 \psi - f^2 \psi \\ \frac{\partial \psi}{\partial n} &= 0 \text{ on } \partial\Gamma \end{aligned} \tag{1}$$

where $\frac{D}{Dt} \equiv \frac{\partial}{\partial t} + \mathbf{u}.\nabla$, q is the quasi-geostrophic potential vorticity, ψ the stream-function, $\mathbf{u} = (u, v)$ the velocity. f the Coriolis parameter, g the acceleration due to gravity, and h_0 a reference value of the fluid depth are all assumed constant. The deformation radius L_R is $\sqrt{g}h_0/f$.

For length scales $L \ll L_R$, equation (1) reduces to

$$\begin{aligned} \frac{Dq}{Dt} &= 0 \\ \mathbf{u} &= (-\frac{\partial \psi}{\partial y}, \frac{\partial \psi}{\partial x}) \\ q &= gh_0 \nabla^2 \psi \\ \frac{\partial \psi}{\partial n} &= 0 \text{ on } \partial\Gamma \end{aligned} \tag{2}$$

This is the standard equation for two-dimensional incompressible flow, with the potential vorticity reducing to the absolute vorticity. The solutions can be analysed by using vorticity conservation, for instance as set out in Gerard (1992). Given initial absolute vorticity which has bounded gradients, we estimate the rate of growth of the vorticity gradients. Differentiating the first equation of (2) gives

$$\frac{D}{Dt}\nabla q + \begin{pmatrix} \frac{\partial u}{\partial x} & \frac{\partial v}{\partial x} \\ \frac{\partial u}{\partial y} & \frac{\partial v}{\partial y} \end{pmatrix} \nabla q = 0 \tag{3}$$

This can be written in terms of the stream-function ψ as

$$\frac{D}{Dt}\nabla q + \begin{pmatrix} -\frac{\partial^2 \psi}{\partial x \partial y} & \frac{\partial^2 \psi}{\partial x^2} \\ -\frac{\partial^2 \psi}{\partial y^2} & \frac{\partial^2 \psi}{\partial y \partial x} \end{pmatrix} \nabla q = 0 \tag{4}$$

These equations can be used to estimate the rate of increase of vorticity gradients, using a bound on the velocity gradients in terms of the vorticity and its gradients (Gerard 1992, p 424):

$$\| \nabla \mathbf{u}(t) \| \leq C \log(2 + \| \nabla q(t) \|) \tag{5}$$

Exact definitions of the norms used are given by Gerard. However, they are essentially maximum norms. The bound is derived from the solution procedure for the Poisson equation for ψ in terms of q. Because of the dependence of the bound in (5) on the vorticity gradients, the estimate of vorticity gradients obtained from (3)

allows exponential growth in time. This does not prevent regularity being proved for all time, but allows the accumulation of enstrophy at small scales. This can be expressed as a statement that

$$\| \nabla \mathbf{u}^2 \| \leq C \| \mathbf{u}^2 \| \tag{6}$$

where C grows exponentially in time. If the L^2 norm is used instead of the maximum norm, then an estimate of the form (6) holds with C independent of time, but dependent on the domain size. Thus the mean scale of the flow is bounded, but local regions where small scales are generated are permitted. This agrees with widespread computational experience.

In the case $L \gg L_R$, equations (1) reduce to the 'equivalent barotropic' equations:

$$\begin{aligned} -f^2 \frac{\partial \psi}{\partial t} + g h_0 \mathbf{u}.\nabla(\nabla^2 \psi) &= 0 \\ \mathbf{u} &= \left(-\frac{\partial \psi}{\partial y}, \frac{\partial \psi}{\partial x} \right) \\ \frac{\partial \psi}{\partial n} &= 0 \text{ on } \partial\Gamma \end{aligned} \tag{7}$$

These equations are less amenable to study than (2), as they cannot be expressed simply as vorticity conservation. This is because the leading order transport term, which would be $-f^2 \mathbf{u} \cdot \nabla \psi$, is zero. It is therefore to be expected that advection will be much less effective at changing the potential vorticity distribution. Larichev and McWilliams (1991) show that the solutions behave very differently from those for two-dimensional incompressible flow. In particular, the spectral shape for the potential enstrophy remains almost invariant in time, with a slow migration to larger scales. There is no cascade to small scales.

We also note at this point an important difference between two-dimensional and three-dimensional quasi-geostrophic flow. If the flow is non-divergent, there is no transfer of energy between potential and kinetic energy in the shallow water equations. If the non-divergent flow is also geostrophic, we can write the kinetic energy as $\frac{1}{2} f^{-2} h (\nabla h)^2$, where h is the fluid depth. In the case where $h - h_0 \ll h_0$, this reduces to $\frac{1}{2} f^{-2} h_0 (\nabla h)^2$. The potential energy is $\frac{1}{2} h^2$. Conservation of the individual parts of the energy then implies that the mean scale of h is also preserved, preventing any upscale cascade. Charney (1971) showed that there could be an upscale cascade for three-dimensional quasi-geostrophic flow, provided the scale was less than L_R. Thus shallow water models cannot be used to study the upscale cascade in h, except on scales small enough for the geostrophic constraint not to be relevant.

2.2 Linear theory

We illustrate the effect of varying the deformation radius by a standard linear analysis. Assume a basic state $\overline{\psi} = -Uy$, implying a geostrophic wind $(U, 0)$ and potential vorticity $\overline{q} = f + f^2 U y$, and linearise (1) about this state, giving:

$$\begin{aligned} \frac{\partial q'}{\partial t} + U \frac{\partial q'}{\partial x} + v' \frac{\partial \overline{q}}{\partial y} &= 0 \\ q' = g h_0 \nabla^2 \psi' - f^2 \psi' & \\ \frac{\partial \psi'}{\partial n} &= 0 \text{ on } \delta\Gamma \end{aligned} \tag{8}$$

Substituting $\psi' = \psi_0 \exp^{i(kx+\omega t)}$ gives

$$-i(\omega+kU)(f^2+gh_0k^2)\psi_0 + ik\psi_0 f^2 U = 0 \tag{9}$$

giving a frequency

$$\omega + kU = \frac{f^2 kU}{(f^2+gh_0k^2)} \tag{10}$$

For scales $L \ll L_R$ we have $\omega \simeq -kU$ and for $L \gg L_R$ we have $\omega \simeq 0$. Thus waves of much shorter wavelength than $2\pi L_R$ translate with the mean flow, and waves with much longer wavelength are stationary.

2.3 Semi-geostrophic theory

Now consider the semi-geostrophic shallow-water model, as used by Cullen (2000). The equations are

$$\begin{aligned}
\frac{Du_g}{Dt} + g\frac{\partial h}{\partial x} - fv &= 0 \\
\frac{Dv_g}{Dt} + g\frac{\partial h}{\partial y} + fu &= 0 \\
\frac{\partial h}{\partial t} + \nabla\cdot(h\mathbf{u}) &= 0 \\
(fv_g, -fu_g) &= g\nabla h \\
\mathbf{u}\cdot\mathbf{n} &= 0 \text{ on } \delta\Gamma
\end{aligned} \tag{11}$$

The suffix g denotes geostrophic values. Following Cullen and Purser (1989), they can be rewritten in geostrophic coordinates (X,Y) in terms of an inverse potential vorticity ρ as

$$\begin{aligned}
\frac{D\rho}{Dt} &= 0 \\
\mathbf{U} &= \left(-\frac{\partial\Psi}{\partial y}, \frac{\partial\Psi}{\partial x}\right) \\
\rho &= \det\frac{\partial^2(\Psi + \frac{1}{2}(X^2+Y^2))}{\partial(X,Y)^2} \\
\nabla\left(\Psi + \frac{1}{2}(X^2+Y^2)\right) &\in \Gamma.
\end{aligned} \tag{12}$$

where $\frac{D}{Dt} \equiv \frac{\partial}{\partial t} + \mathbf{U}\cdot\nabla$; and $\mathbf{U} = (U,V)$ and Ψ are the velocity and stream function with which the inverse potential vorticity is transported in geostrophic coordinates. The solution for $\mathbf{x}$ in terms of $\mathbf{X}$ can be described in terms of minimising the energy:

$$E = \frac{1}{2}f^2 \int_\Gamma \left((x-X)^2 + (y-Y)^2\right) d\tau \tag{13}$$

with respect to incompressible particle displacements conserving ρ. These displacements can be interpreted as area-preserving displacements of $\mathbf{x}$ for fixed $\mathbf{X}$. An equation of the form (4) still governs the rate of growth of inverse potential vorticity gradients. Using (12), we obtain

$$\frac{D}{Dt}(\nabla\rho)+\begin{pmatrix} -\frac{\partial^2\Psi}{\partial X\partial Y} & \frac{\partial^2\Psi}{\partial X^2} \\ -\frac{\partial^2\Psi}{\partial Y^2} & \frac{\partial^2\Psi}{\partial Y\partial X}\end{pmatrix}\nabla\rho=0 \tag{14}$$

The equation that determines Ψ from ρ is a Monge-Ampere equation for $R=\Psi+\frac{1}{2}(X^2+Y^2)$. R has to be a convex function. Thus ρ is transported by a flow generated by the difference between a convex stream-function and a solid-body rotation. If the flow is steady, particles move along streamlines. Convexity prevents streamlines converging exponentially, and thus exponential growth of gradients of ρ, except over distances short compared with the length of a streamline. Only algebraic growth is permitted, controlled by the rate of increase of $\mathbf{U}$ with distance from the centre of rotation.

In the unsteady case, consider a closed loop S in the fluid, with scalar line element ds. Then we can cyclically displace $\mathbf{x}$ by a distance ds around the loop, which changes the local value of $\mathbf{x}$ by an amount $(d\mathbf{x}/ds)ds$, giving

$$\delta E=f^2\int_S(\mathbf{x}-\mathbf{X})\cdot\frac{d\mathbf{x}}{ds}ds \tag{15}$$

This has to be zero because the solution for $\mathbf{x}$ in terms of $\mathbf{X}$ represents an energy minimising state. Writing $\mathbf{U}=f(y-Y,X-x)$, (15) can therefore be written

$$\delta E=\int_S\frac{d\mathbf{U}}{ds}\cdot(\mathbf{U}ds)=0 \tag{16}$$

The rate of extension of the loop can be written

$$\frac{d|S|}{dt}=\int_S\frac{d\mathbf{U}}{ds}\cdot d\mathbf{X} \tag{17}$$

Comparing (16) with (17) shows that there can be no growth of the line element coming from the parts with $d\mathbf{X}$ correlated with $\mathbf{U}$. Thus the normal straining mechanism leading to the enstrophy cascade is excluded. Growth is possible from the parts of the line element uncorrelated with $\mathbf{U}$. This will normally be algebraic growth only, as in the steady case. Transient exponential growth is possible if the time evolution changes the velocity field in a way that the line element does not align to it as it grows. Thus the exponential growth of line elements, as observed in normal two-dimensional turbulence, is inhibited in the semi-geostrophic case, but it is not at present possible to exclude it altogether.

3 Numerical results

3.1 Dynamical core experiments

We first show the results of a dynamical core experiment using the ECMWF model at a resolution of T_L95L50. This is an important illustration because the upscale cascade in the stream-function in quasi-geostrophic theory can only occur in the three-dimensional case. The experiment was carried out using the standard procedure defined by Held and Suarez (1994). In particular, the only physical 'forcing' is zonally symmetric. Fig.3

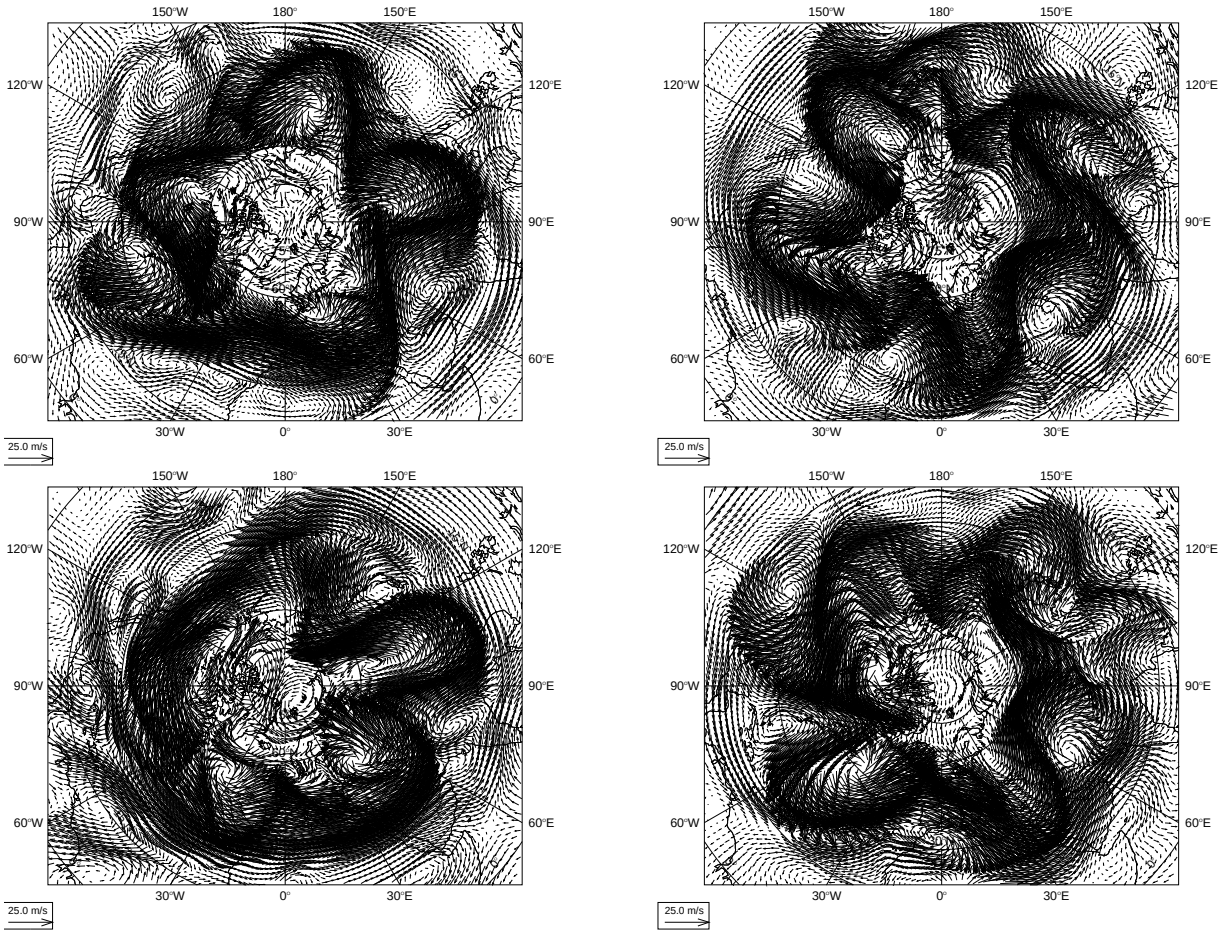

Figure 3: Wind fields at model level 39 (around 500hpa) at 100 day intervals from a dynamical core experiment with the ECMWF model.

shows the winds near 500hpa at 100-day intervals, showing that non-zonal eddies persist even in the absence of asymmetric forcing. There is no sign of an inverse cascade taking the height field towards a zonal state. The scale of the eddies will be primarily set by baroclinic instability and is therefore equal to the effective L_R for the flow. We can say that the inverse cascade appears to be absent for scales larger than L_R.

3.2 Shallow water models and experimental design

The models used for this study are two of the models used by Cullen (2000) to study the accuracy of the semi-geostrophic approximation. They are spherical models. For the purposes of this study, the Coriolis parameter was set to a constant value at all points in order to ensure uniformity of the radius of deformation. Inclusion of the correct variation of the Coriolis parameter would have obscured the issues studied in this paper. The semi-geostrophic model is that described and used by Mawson (1996). It uses equations (11), semi-Lagrangian advection of the primitive variables (u_g, v_g, h), and an implicit method of calculating (u, v) to ensure that the geostrophic relation is satisfied at each new time level. The variables (h, u, v) are stored on a C grid, and

(u_g, v_g) are held on a D grid. The implicit equations are solved by a multigrid method. The data are initialised by first choosing analytic height and geostrophic wind fields, and then carrying out the discrete initialisation procedure set out in Mawson (1996). The initial values of u and v are set by making an initial time step, and calculating the u and v needed to preserve geostrophic balance. The primitive equation model is a shallow water version of the semi-implicit version of the UK Meteorological Office model (Cullen et al. (1997)). It uses a C grid, semi-Lagrangian advection, and multigrid solution of the implicit equations. Both models were run on a latitude-longitude grid with 288×193 points.

In order to show the effect of the deformation radius, we use two values for the mean fluid depth, $gh_0 = 10^5 m^2 s^{-2}$ and $5000 m^2 s^{-2}$. We set the Coriolis parameter equal to its North Pole value of $1.458_{10} - 4$. The equivalent deformation radii are 2148 and 480km respectively. At the equator, these correspond to wavenumbers 3 and 13.3. We use test data with a spread of zonal wavenumbers between 3 and 19. The perturbations are thus mainly on scales less then L_R in the first case, and greater than L_R in the second case. The amplitudes of the depth perturbations are chosen to give roughly equal potential vorticity perturbations at each wavenumber in the case where the depth perturbations are small compared with the mean depth. The amplitudes are such that, in the case with $gh_0 = 5000 m^2 s^{-2}$, the maximum and minimum depths are 825m and 154m and are thus large compared with the mean depth of 510m. The initial depth field is shown in Fig.4.

The choice of changing L_R by changing the mean depth means that the velocity fields and height gradients are the same in both experiments. Since the initial rate of extension of line elements and increase of potential vorticity gradients depends on the velocity field, this gives the closest comparison between the two cases. The potential vorticity distribution is not the same, because the variations of the factor $1/h$ are large when the smaller mean depth is used. Fig.4 shows the initial semi-geostrophic and Ertel potential vorticities in the case $gh_0 = 10^5 m^2 s^{-2}$. Since most of the structure is on a scale less than L_R, the two fields are not very similar. Fig.5 shows the semi-geostrophic and Ertel potential vorticities in the case $gh_0 = 5000 m^2 s^{-2}$. There is now a strong correlation with the depth field, as expected and the two forms of potential vorticity now have a very similar distribution.

3.3 Results from the shallow water models

We first show results from 20 day integrations using $gh_0 = 10^5$. Fig. 6 shows the final depth fields, which are very similar to each other, and dominated by the same scales of perturbations as the initial data. This is consistent with the expected conservation of the mean scale of the depth field in two-dimensional quasi-geostrophic flow. The depth field given by the primitive equation model is slightly smoother. The numerical methods are the same in both models, so cannot explain the difference. A possibility is that the primitive equation model can use gravity waves to disperse numerical errors, while the semi-geostrophic model cannot. The result may also indicate that an upscale cascade is operating at the smaller scales, where the geostrophic approximation is less accurate.

Fig. 7 shows time-series of diagnostics from the integrations. We plot the potential and kinetic energies, the potential enstrophy, the H^1 norm of the velocity, defined by

$$\int\int \frac{1}{a\cos\phi}\left[\left(\frac{\partial u}{\partial\lambda} - v\sin\phi\right)^2 + \left(\frac{\partial u\cos\phi}{\partial\phi}\right)^2 + \left(\frac{\partial v}{\partial\lambda} + u\sin\phi\right)^2 + \left(\frac{\partial v\cos\phi}{\partial\phi}\right)^2\right] d\lambda d\phi \qquad (18)$$

and the H^1 norm of the potential vorticity, defined by

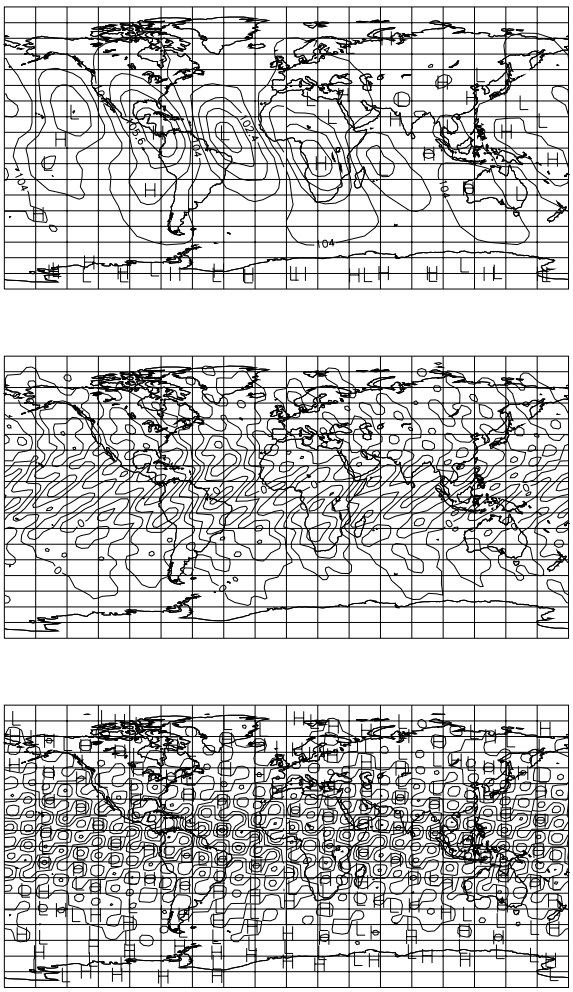

Figure 4: Initial fields for shallow water experiments with $gh_0 = 10^5$. Top: depth field (units 10^2m, contour interval 80m). Centre: Ertel potential vorticity (units $(\mathrm{ms})^{-1}$, contour interval $0.3_{10} - 9$. Bottom: semi-geostrophic potential vorticity (units 10^{-13} $\mathrm{m}^{-1}\mathrm{s}^{-2}$, contour interval 1.0.

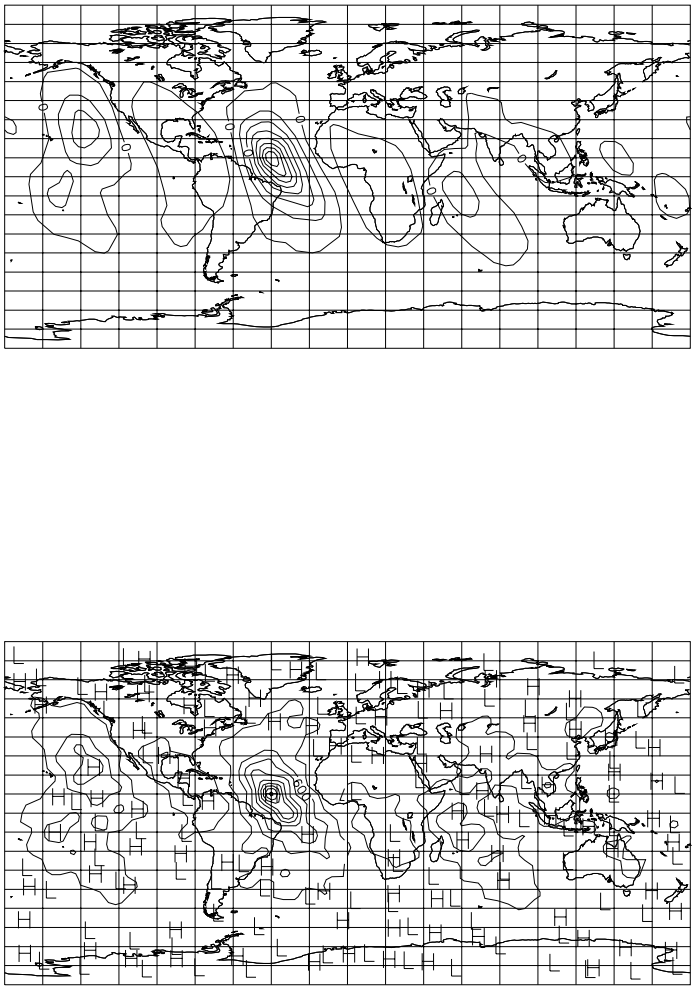

Figure 5: Initial fields for shallow water experiments with $gh_0 = 5000$. Top: Ertel potential vorticity (units $(\mathrm{ms})^{-1}$, contour interval $0.8_{10} - 7$. Bottom: semi-geostrophic potential vorticity, (units 10^{-13} $\mathrm{m}^{-1}\mathrm{s}^{-2}$, contour interval 150.0.)

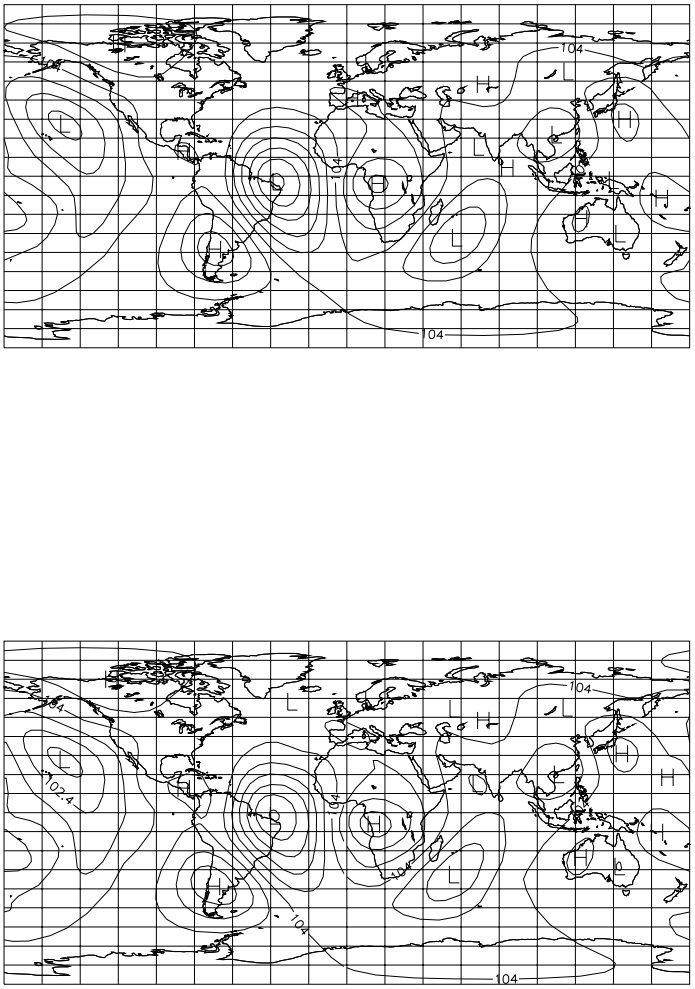

Figure 6: Depth fields after 20 days of time integration with $gh_0 = 10^5$: top: primitive equation model, bottom: semi-geostrophic model. Units 10^2m, contour interval 80m.

$$\int\int \frac{1}{a}\left[\left(\frac{\partial q}{\cos\phi\partial\lambda}\right)^2+\left(\frac{\partial q}{\partial\phi}\right)^2\right]\cos\phi d\lambda d\phi \tag{19}$$

In these equations λ,ϕ are longitude and latitude, and a is the radius of the sphere. The appropriate potential vorticity is shown for each model. Each quantity is scaled by its initial value.

These diagnostics show good conservation of the potential enstrophy and total energy. These should be conserved by both models, but neither numerical method exactly conserves either quantity. Thus the overall conservation is a good check on numerical accuracy. The kinetic energy drops slowly, losing about 16% of its value over 20 days in the primitive equation model and 9% in the semi-geostrophic model. These relatively small changes are consistent with the conservation of the mean scale of the depth field. The H^1 norm of the velocity field is not so well conserved. The argument for conservation of the mean scale of the velocity field assumes that potential enstrophy conservation constrains all the velocity gradients. Even in the non-divergent case this constraint is not sufficient, because the potential vorticity only involves a particular linear combination of gradients. The results show a decrease of 58% and 41% in this norm in the primitive equation and semi-geostrophic case respectively. This implies an increase in the mean scale of the velocity field.

In the primitive equation model there is a rapid increase in potential vorticity gradients, as measured by the H^1 norm. This is consistent with an enstrophy cascade. After 3 days the rise stops, and values then fall. Maps of potential vorticity late in the run show very little structure. The obvious explanation is that the scale collapse associated with the increasing gradients means that the solution is no longer resolved after day 3 and the potential vorticity distribution thereafter is just numerical noise. This is the message of experiments carried out with contour advection methods, e.g. Dritschel and Ambaum (1997). In the semi-geostrophic integration, the rise in the H^1 norm of the potential vorticity is much slower. The peak value is less than half that in the primitive equation integration, and it takes 6 days to reach it, twice as long as in the primitive equation integration. Maps of the potential vorticity even after 20 days show considerable structure.

We therefore study the first two days of these integrations more closely, for which time the potential vorticity field should be reasonably resolved. In Fig. 8 we show graphs of the H^1 norm of the potential vorticity for the two models. In addition, we show graphs using two additional initial data sets. The second dataset is only different from the first in the higher wavenumbers (greater than zonal wavenumber 3). The third dataset has a wavenumber 2 perturbation instead of a wavenumber 3 perturbation. The difference in the behaviour of the models is consistent, so we can safely conclude that the enstrophy cascade is inhibited in the semi-geostrophic model. The use of a wavenumber 2 rather than a wavenumber 3 perturbation changes the answers significantly, reducing the difference between the two models. This is to be expected, as the deformation radius corresponds to wavenumber 3. Fig. 9 shows the potential vorticity distributions after 2 days for the original data. We can see that the stretching is significantly greater in the primitive equation integration..

We next show results from the case $gh_0 = 5000$. Fig.10 shows time series of the same diagnostics as plotted in Fig.7. The kinetic energy changes are similar to those in the case $gh_0 = 10^5$. The decrease in the H^1 norm of the velocity is somewhat less, being 45% in the primitive equation model and 30% in the semi-geostrophic model. The rate of increase and the maximum relative value of the H^1 norm of the potential vorticity are much less. The primitive equation model still reaches its peak value at 2 days, much earlier than in the semi-geostrophic model. Thus there is a general suppression of the enstrophy cascade, and the difference between the two models is smaller.

In Fig. 11 we show the potential vorticity distributions after 2 days. The character of the fields is completely different from Fig. 9, as expected from the differences in the initial data shown in Figs. 4 and 5. The difference between the two models is much less apparent than with the larger value of mean depth.

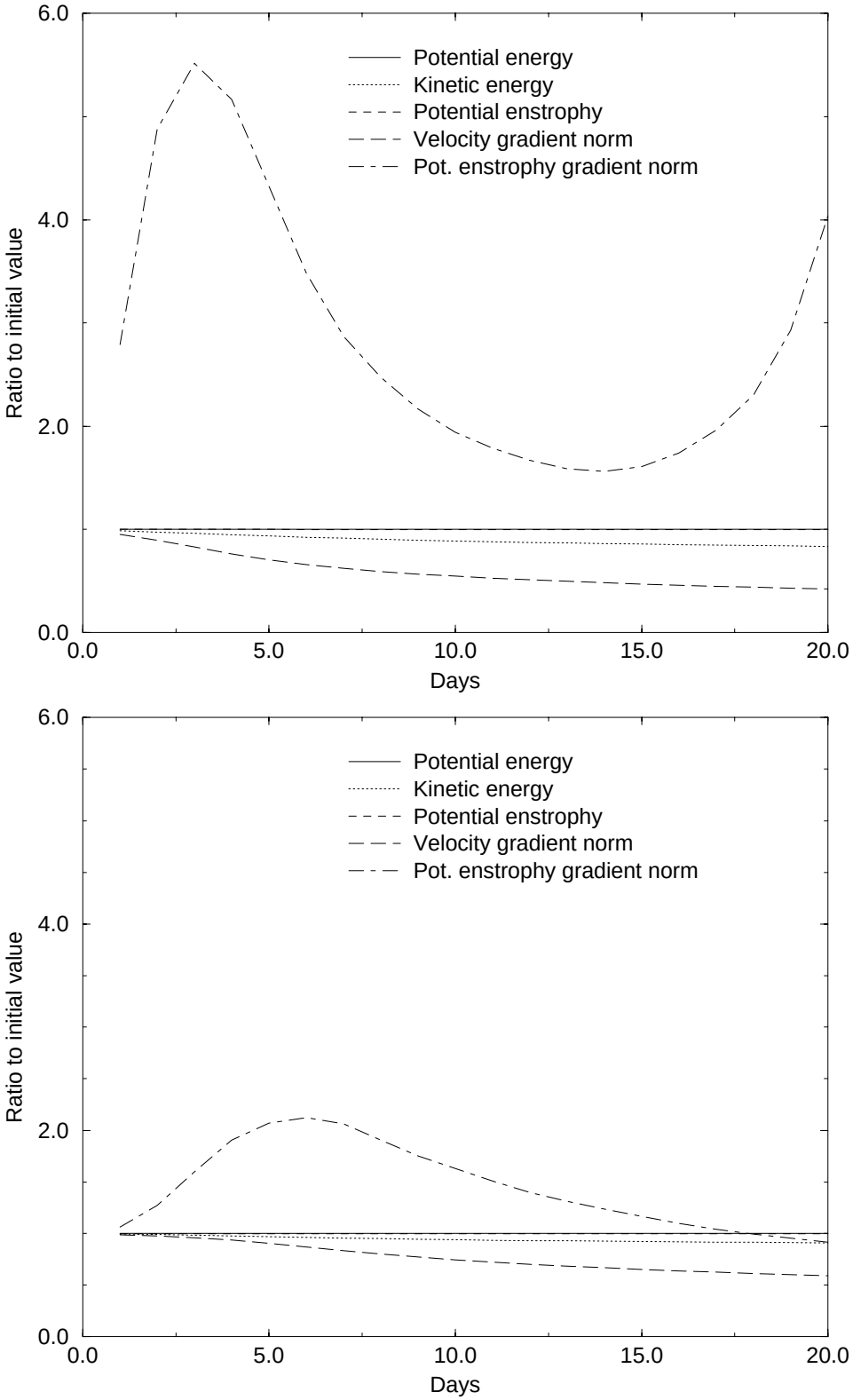

Figure 7: Graphs of diagnostics from integration of (top) primitive equation model and (bottom) semi-geostrophic model against time. $gh_0 = 10^5$.

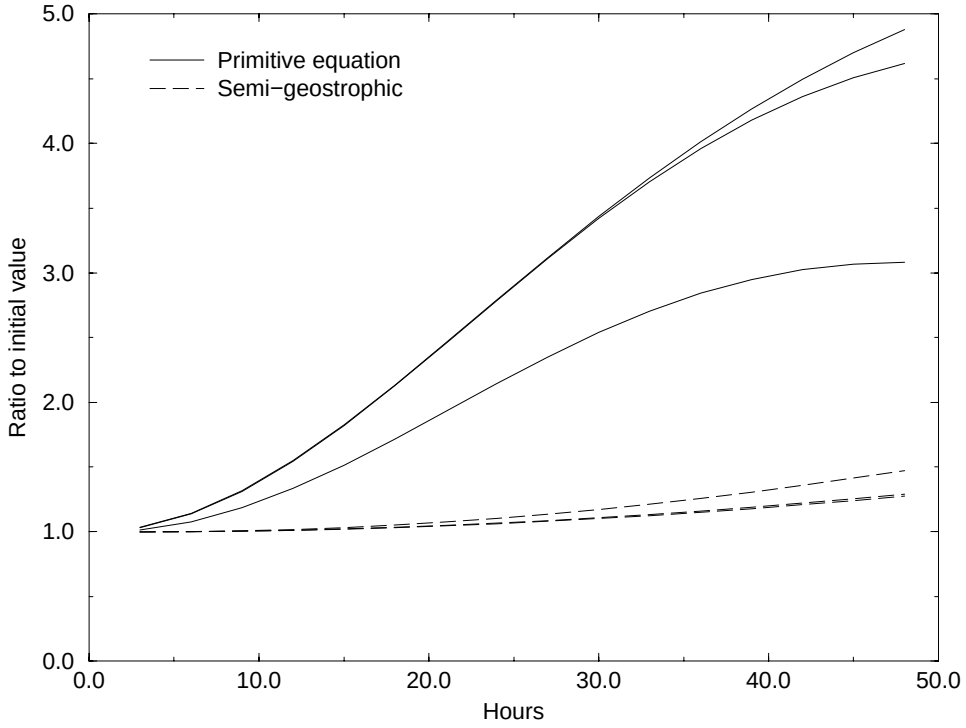

Figure 8: Graphs of the potential enstrophy gradient norm from integrations of primitive equation and semi-geostrophic models against time for the first two days of integration using three different initial data sets.

4 Discussion

The main results of this paper are to reinforce earlier work that demonstrates the qualitative change in potential vorticity dynamics between the cases $L < L_R$ and $L > L_R$. The strong correlation of potential vorticity with depth, rather than with relative vorticity, is clearly seen in the case $L > L_R$. The cascade of enstrophy to small scales is inhibited in this case. The extra constraints applying to two-dimensional quasi-geostrophic flow mean that the inhibition of the upscale cascade in the depth field can only be demonstrated in a three-dimensional experiment such as the dynamical core experiment. Since the active scales in extra-tropical synoptic flow are equal to or greater than L_R, the internal dynamics can be considered non-cascading and essentially non-turbulent, as observed.

We have also shown that the enstrophy cascade is inhibited in the semi-geostrophic model. This is consistent with the accuracy of this model for scales larger than L_R and inaccuracy for scales smaller than L_R. Since the condition for semi-geostrophic theory to be accurate only requires that only one horizontal scale is larger than L_R, the creation of filamentary structures can be accurately described. However, they may be unrealistically stable.

These results are very clear-cut, and reproducible with different choices of initial data. Though it would have been ideal to use a contour dynamics code for the study, sufficient resolution was maintained for long enough for the conclusions to be considered reliable.

The large differences between the potential vorticity dynamics in the two shallow water models has little impact

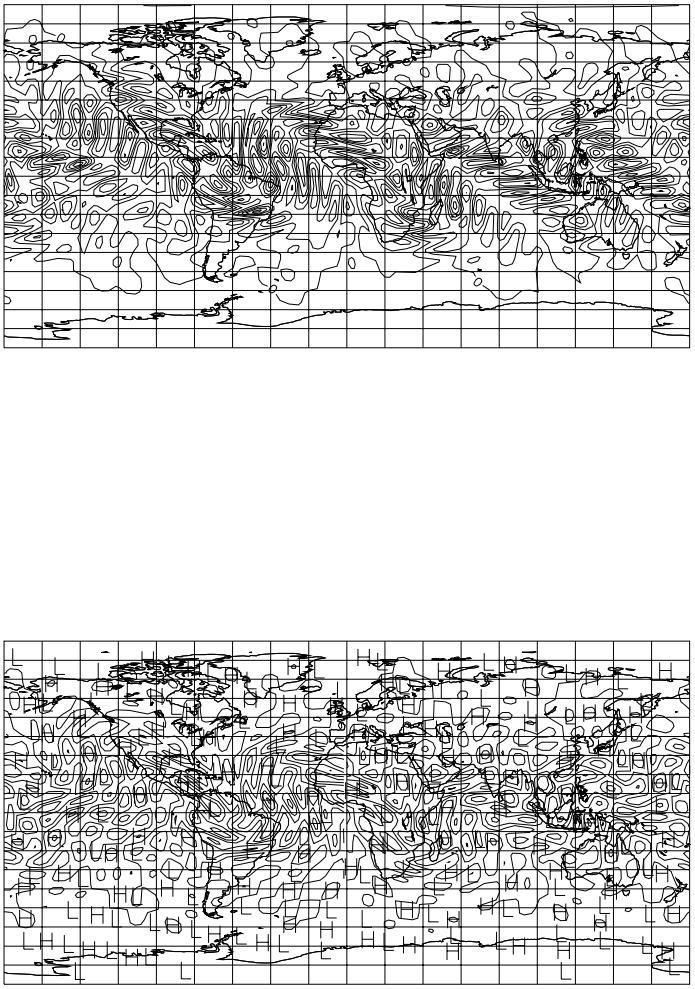

Figure 9: Potential vorticity distributions after 2 days with $gh_0 = 10^5$ for: top, primitive equation model; bottom; semi-geostrophic model. Units and contour intervals as Fig.4

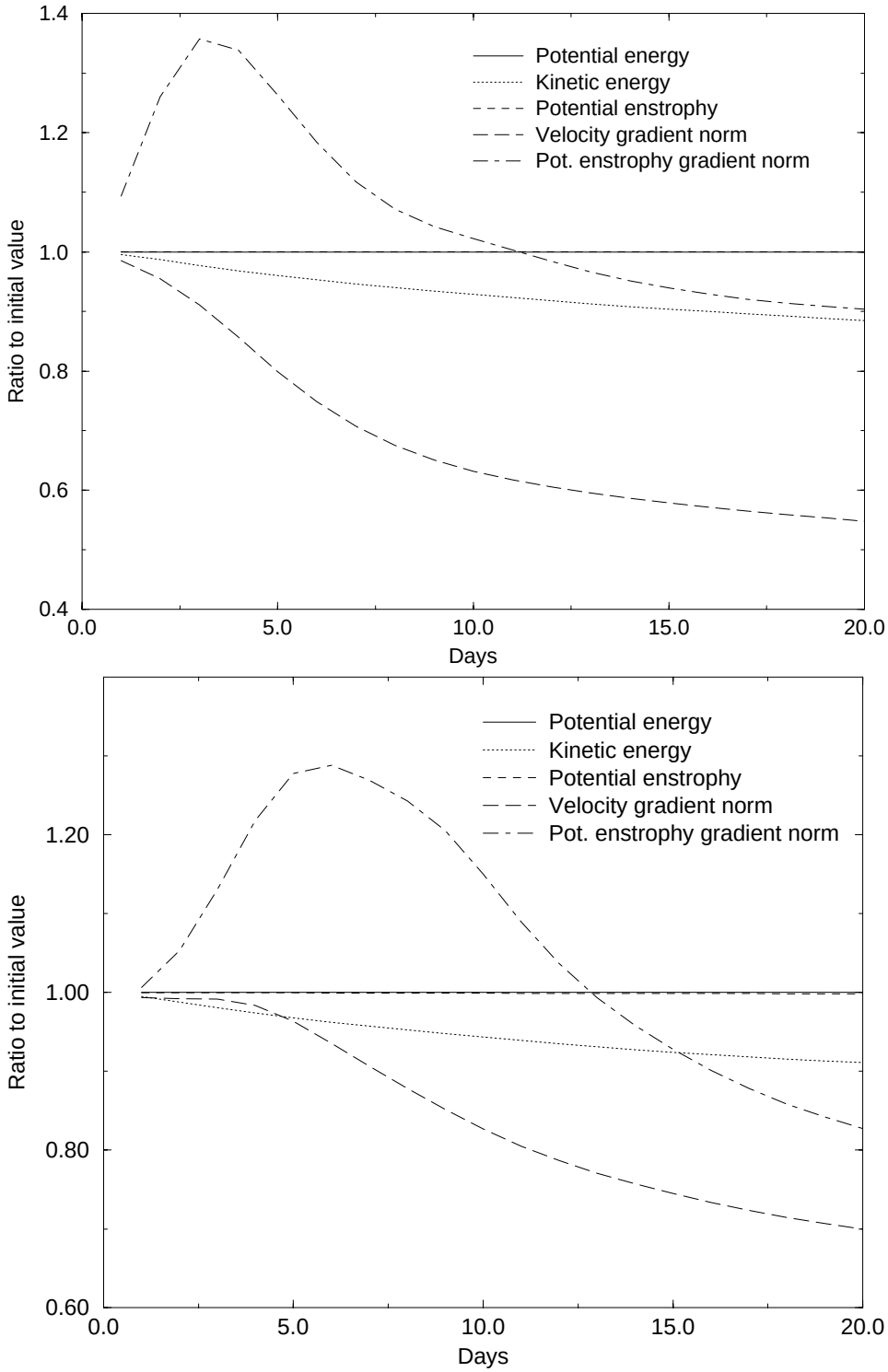

Figure 10: Graphs of diagnostics from integration of (top) primitive equation model and (bottom) semi-geostrophic model against time. $gh_0 = 5000$.

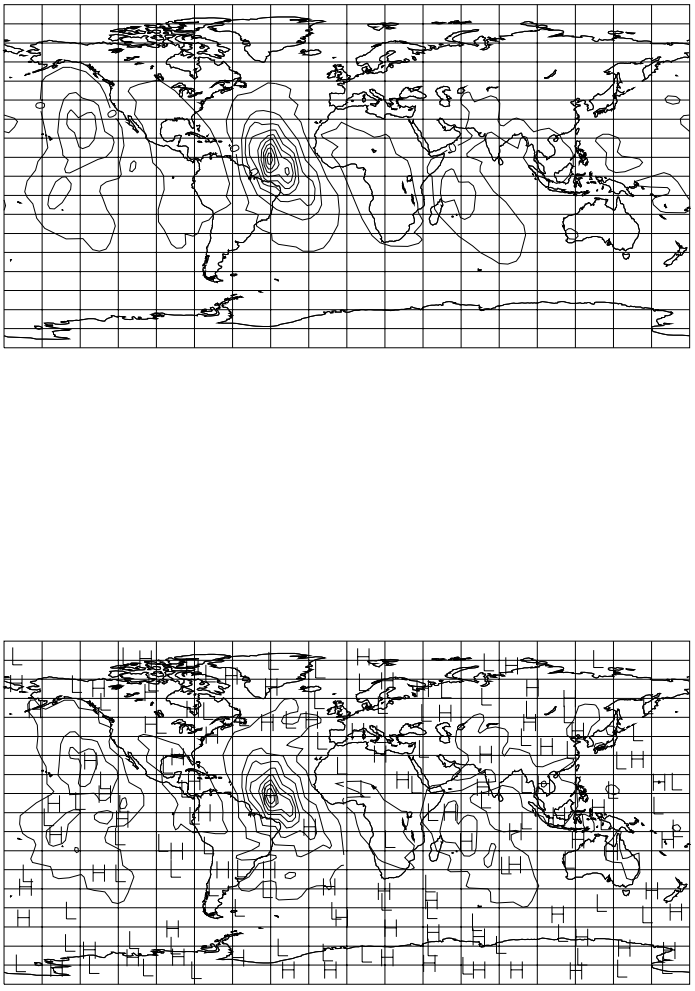

Figure 11: Potential vorticity distributions after 2 days with $gh_0 = 5000$ for: top, primitive equation model; bottom; semi-geostrophic model. Units and contour intervals as Fig.5

on forecasts of the depth field. This is consistent with the finding of Methven and Hoskins (1998) that forecasts of pressure and wind fields were very insensitive to increases in model resolution which improved the description of the potential vorticity evolution. Potential vorticity dynamics is important as an indicator of how well tracers are transported. It is therefore important to determine whether observed potential vorticity filaments are primarily visible as changes in the thickness of isentropic layers, or as relative vorticity filaments. In the former case, the mixing may be much less efficient than suggested by classical two-dimensional turbulence.

Acknowledgements

The theoretical part of the work was done during the Isaac Newton Institute programme on the 'Mathematics of Atmosphere Ocean Dynamics', held from June to December 1996. The author wishes to thank Mariano Hortal for providing the dynamical core results, various staff at the U.K. Meteorological Office for providing the shallow water codes used in the study, Robert Douglas for some revisions to the theoretical section, and Deborah Salmond for reviewing the manuscript.

References

Charney,J.G. (1971): Geostrophic Turbulence; *J. Atmos. Sci.*, **28**, 1087-1095.

Charney,J.G. and Devore,J. (1979): Multiple flow equilibria in the atmosphere and blocking; *J. Atmos. Sci.*, **36**, 1205-1216.

Cullen,M.J.P. (2000): On the accuracy of the semi-geostrophic approximation. *Quart. J. Roy. Meteor. Soc*, **126**, 1099-1115.

Cullen,M.J.P., Davies,T., Mawson,M.H., James,J.A. and Coulter,S. (1997): An overview of numerical methods for the next generation UK NWP and climate model; in 'Numerical Methods in Atmosphere and Ocean Modelling', The Andre Robert Memorial Volume. (C.Lin, R.Laprise, H.Ritchie, Eds.), Canadian Meteorological and Oceanographic Society, Ottawa, Canada, 425-444.

Cullen,M.J.P. and Purser,R.J. (1989): Properties of the Lagrangian semi-geostrophic equations; *J. Atmos. Sci.*, **46**, 2684-2697.

Dritschel,D.G. and Ambaum,M.H.P. (1997): A contour-advective semi-Lagrangian numerical algorithm for simulating fine-scale conservative numerical fields; *Quart. J. Roy. Meteor. Soc*, **123**, 1097-1130.

Farge,M. and Sadourny,R. (1989): Wave-vortex dynamics in rotating shallow water; *J. Fluid Mech.*, **206**, 433-462.

Gage,K.S. and Nastrom,G.D. (1986): Theoretical interpretation of atmospheric wavenumber spectra of wind and temperature observed by commercial aircraft during GASP; *J.Atmos. Sci.*, **43**, 729-740.

Gerard,P. (1992) Resultats recents sur les fluides parfaits incompressibles bidimensionnels; *Seminaire Bourbaki*, **757**, 411-444.

Held,I.M. and Suarez,M.J. (1994): A proposal for the intercomparison of the dynamical cores of atmospheric general circulation models; *Bull. Am. Meteor. Soc.*, **73**, 1825-1830.

Holloway,G. (1986): Eddies, waves, circulation, and mixing: statistical geofluid mechanics; *Ann. Rev. Fluid Mech.*, **18**, 91-147.

Kato,T. and Ponce,G. (1986): Wellposed-ness of the Euler and Navier-Stokes equations in Lebesgue spaces $L_s^p(\mathcal{R}^2)$; *Rev. Mat. Iberoamerica*, **2**, 73-88.

Larichev,V.D. and McWilliams, J.C. 1991: Weakly decaying turbulence in an equivalent-barotropic fluid; *Phys. Fluids*, **A 3(5)**, 938-950.

Leith,C.E. (1971): Predictability and two-dimensional turbulence; *J. Atmos. Sci.*, **28**, 145-161.

Malardel,S., Joly,A., Courbet,F. and Courtier,Ph. (1993): Nonlinear evolution of ordinary frontal waves induced by low-level potential vorticity anomalies; *Q. J. Roy. Meteor. Soc.*, **119**, 681-713.

Mawson,M.H. (1996): A shallow water semi-geostrophic model on a sphere; *Quart. J. Roy. Meteor. Soc.*, **122,** 267-290.

Methven,J. and Hoskins, B.J. (1998) Spirals in potential vorticity. Part I; measures of structure; *J. Atmos. Sci.*, **55**, 2053-2066.